Motional narrowing in the time-averaging approximation for simulating two-dimensional nonlinear infrared spectra

Motional narrowing in the time-averaging approximation for simulating two-dimensional nonlinear infrared spectra

Thomas la Cour Jansen[1,a] and Wioletta M. Ruszel[2]
[1]*Institute for Theoretical Physics and Zernike Institute for Advanced Materials, University of Groningen, Nijenborgh 4, 9747 AG Groningen, The Netherlands*
[2]*Institute for Mathematics and Computing Sciences, University of Groningen, Nijenborgh 9, 9747 AG Groningen, The Netherlands*

(Received 18 February 2008; accepted 30 April 2008; published online 3 June 2008)

The diagonal linewidth in two-dimensional infrared spectra is often narrower than the distribution of transition frequencies. The width along the antidiagonal is broader than predicted by the lifetime broadening. These effects arise from time-dependent fluctuations of the transition frequencies. They can be accounted for with a semiclassical approach. For systems with many coupled vibrational modes, this approach, however, becomes computationally too demanding to be practically applicable. A time-averaging approximation was suggested for linear infrared absorption spectra. In this paper, we demonstrate that the averaging can be optimized to fit a broader scale of frequency fluctuations by using a Gaussian weight function instead of the originally proposed box function. We further generalize the time-averaging method to allow the simulation of two-dimensional infrared spectra and demonstrate the method on a simple system. The approximation delivers a large speed-up of the calculation without losing significant accuracy. © *2008 American Institute of Physics*. [DOI: 10.1063/1.2931941]

I. INTRODUCTION

Our ability to synthesize and manipulate increasingly more complex molecular systems is continuously growing. In recent years, systems such as molecular motors,[1] proteins, dendrimers,[2] and light-harvesting complexes[3] have been subject to extensive research. In many of these systems, we not only wish to know about or control the structure but also the dynamics on a microscopic scale. To achieve this one needs a method to follow the dynamics on the time scale that it happens. Two-dimensional infrared (2DIR) spectroscopy is such a method with great potential in resolving structure and dynamics down to the femtosecond time scale in complex molecular systems.[4–8] 2DIR has therefore been applied in the study of protein folding processes,[9,10] ultrafast chemical exchange,[11,12] molecular machines,[13] and liquid dynamics.[14] Experimentally complex systems involving numerous coupled vibrations can easily be studied using 2DIR. For example, spectra have been obtained for the amide I band of complex protein structures where hundreds of coupled carbonyl stretch vibrations contribute to the spectra.[15] When the frequencies of the individual vibrations change more slowly than the dephasing time arising from the presence of different vibrations with slightly different frequency, one can safely assume that the frequencies are fixed in time. When dynamical effects can be neglected, the 2DIR spectra can be essentially seen as the joint distribution functions of the frequencies present in the system.[16] This is called the inhomogeneous or static limit. In this limit approximations can be made that allow the calculation of 2DIR spectra of systems with up to a few hundred coupled vibrations.[17–19] The real reason for using 2DIR spectroscopy is, however, the possibility to study dynamics. These effects can be accounted for by computational methods as the numerical integration of the Schrödinger equation (NISE).[20–23] These methods are computationally very demanding and effectively limited to systems with a much smaller number of coupled vibrations.[20,24]

A time-averaging approximation (TAA) was suggested to account for dynamic effects in linear absorption spectra.[25,26] Fast fluctuations of the transition frequencies lead to narrowing of the absorption lines, which can effectively be described by an averaging over the frequencies for a time comparable to the inhomogeneous dephasing time.

In many cases dynamic effects do play a significant role. 2DIR spectra are motionally narrowed by dynamics which average over the frequencies observed in the spectrum. Furthermore, mode mixing leading to population transfer is observed as well. Apart from the NISE approach[20–22] mentioned earlier, several methods have been developed to treat these types of effects both for the 2DIR and the corresponding electronic spectra. Examples are methods based on solving the low-temperature corrected quantum Fokker–Planck equation,[27,28] numerical propagation of the density matrix,[29] combined cumulant expansion with exciton transfer models,[30,31] and solving the stochastic Liouville equation.[22,32] These methods have all been successfully applied to small systems involving a few chromophores. They are, however, all very computationally demanding and cannot be applied to large complex systems.

The methods mentioned earlier are even relatively slow for small systems and therefore not particularly suited for fitting experimental spectra. It typically takes hours to calculate the 2DIR spectrum even for small systems. The possibility of performing such fits is essential for extracting de-

[a]Electronic mail: thomas.lacour@gmail.com.

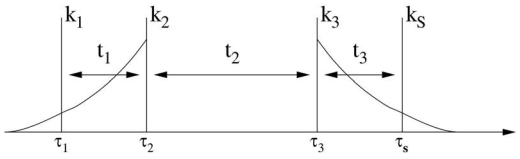

FIG. 1. Timeline for the two-dimensional infrared experiment. The vertical lines marked with k_1, k_2, k_3, and k_S, indicate the interactions with the laser pulses. The time periods t_1 and t_3 are those approximated by averages in the presented method. The decaying lines indicate the backward and forward averages accounting for the motional narrowing taking place in these time intervals.

tailed information from, for example, ultrafast chemical exchange experiments.[11,12,16,32–35] These challenges call for the development of computationally efficient approximate methods that can be applied in fitting procedures.

In this paper we will extend the time-averaging approximation suggested for calculating linear spectra[25] in two ways. First, we will show that using a Gaussian weighting of the averaging improves the accuracy of the approximation and makes it applicable for a broader range of spectral diffusion time scales. Second, we will generalize the method to allow calculating the 2DIR spectra as well.

The remainder of this paper is organized as follows. In Sec. II we will present the theory for the time-averaging approximation. In Sec. III we will demonstrate how the approximation works for a typical model system as well as for the Trpzip2 β-hairpin peptide. Finally, we will draw the conclusions in Sec. IV.

II. THEORY

We employ the simplest possible exciton Hamiltonian for a collection of N floating anharmonic oscillators of the form

$$\mathbf{H}(t) = \sum_{i=1}^{N} \left[\epsilon_i(t) \boldsymbol{b}_i^\dagger \boldsymbol{b}_i - \frac{\Delta_i(t)}{2} \boldsymbol{b}_i^\dagger \boldsymbol{b}_i^\dagger \boldsymbol{b}_i \boldsymbol{b}_i \right] + \sum_{i,j=1}^{N} J_{ij}(t) \boldsymbol{b}_i^\dagger \boldsymbol{b}_j + \sum_{i=1}^{N} \vec{\mu}_i(t) \cdot \vec{E}(t) [\boldsymbol{b}_i^\dagger + \boldsymbol{b}_i]. \quad (1)$$

Here $\epsilon_i(t)$ and $\Delta_i(t)$ are the fluctuating frequency and anharmonicity of mode i, respectively. $J_{ij}(t)$ is the coupling between two modes which may depend on time. $\boldsymbol{b}_i^\dagger$ and $\boldsymbol{b}_i$ are the usual Bose creation and annihilation operators. The modes interact with the applied infrared electric field $\vec{E}(t)$ through the transition dipoles $\vec{\mu}_i(t)$ which might fluctuate in time as well.

The pulse sequence for the nonlinear two-dimensional infrared experiment is given in Fig. 1. The first pulse with wave vector $\vec{k}_1$ brings the system into a coherent superposition between the ground state and a single excited state. After a time t_1 the second pulse with wave vector $\vec{k}_2$ brings the system either back to the ground state or into a single excited state population. The system is allowed to relax during the waiting time t_2. Then it is brought into a coherent superposition between a single excited state and either the ground state or a double excited state. Finally, the signal is collected by measuring the light emitted in the directions $\vec{k}_S^{\mathrm{I}} = -\vec{k}_1 + \vec{k}_2 + \vec{k}_3$ (photon echo/rephasing) and $\vec{k}_S^{\mathrm{II}} = \vec{k}_1 - \vec{k}_2 + \vec{k}_3$ (nonrephasing) and adding the two to obtain the absorptive nonlinear two-dimensional infrared signal. There are six contributions to the signal which are illustrated by their Feynman diagrams in Fig. 2.[36] These are the ground state bleach, the stimulated emission, and the excited state absorption signals which all have both a rephasing and a nonrephasing part.

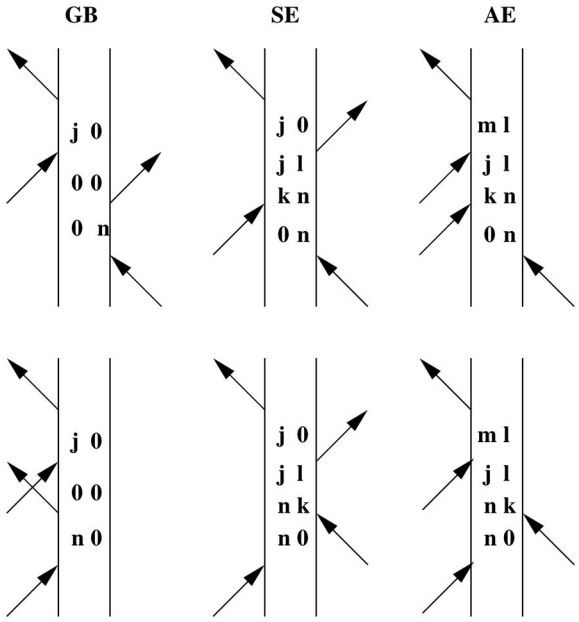

FIG. 2. Feynman diagrams for the six contributions to the two-dimensional infrared spectrum (Ref. 36). The upper row contains the rephasing diagrams and the lower row contains the nonrephasing diagrams. n, j, k, and l denote single excited states, while m denotes a double excited state. During t_2 population/coherence transfer between single excited states can occur in the stimulated emission (SE) and excited state absorption (EA) diagrams, while this does not occur in the ground state bleach diagrams (GB).

By varying the waiting time t_2, many interesting processes as rotational motion, population transfer, spectral diffusion, and chemical exchange can be observed. The time periods t_1 and t_3 predominantly give rise to motional narrowing. When one is most interested in the processes taking place during t_2, it is reasonable to look for an efficient approximation of the motional narrowing taking place during the other time delays. We will demonstrate that by such approximations a substantial speed-up can be gained, with only a small loss in the accurate description of the line shape as provided by the full simulations in for example the NISE method.[21]

As it will turn out the motional narrowing during t_1 effectively corresponds to averaging the fluctuating Hamiltonian [Eq. (1)] from the arrival of the second pulse and backward in time as illustrated in Fig. 1. In the same way the motional narrowing during time t_3 will be accounted for by forward averaging after the third pulse, also illustrated in Fig. 1. In the following the derivation of the time-averaging approximation from the NISE expressions will be discussed.

A. The time-averaging approximation

In the NISE scheme[21] the linear absorption is given by

$$I(\omega) = \Im \int_0^\infty \sum_{j,k} \exp(-i\omega t - t/2T_1)\langle \mu_j(t) U_{jk}(t,0)\mu_k(0)\rangle dt. \tag{2}$$

T_1 is the vibrational lifetime and $\langle \cdots \rangle$ denotes the ensemble average. The variables j and k run over the single excited states. $U_{j,k}(t,0)$ is the solution of the time-dependent Schrödinger equation in the time interval from 0 to t. This solution can be written as

$$U_{jk}(t,0) = \left\{ \exp_T \left[-\frac{i}{\hbar} \int_0^t \boldsymbol{H}(\tau) d\tau \right] \right\}_{jk}, \tag{3}$$

where $\exp_T$ is the time ordered exponential.[36] This can be rewritten in terms of the average of the Hamiltonian in the time interval from 0 to t,

$$U_{jk}(t,0) = \left\{ \exp_T \left[-\frac{it}{\hbar} \frac{1}{t} \int_0^t \boldsymbol{H}(\tau) d\tau \right] \right\}_{jk}. \tag{4}$$

Auer and Skinner suggested approximating this expression by using the average over a fixed time interval T.[25] We will allow using a slightly more general average introducing a weight function. The reason for doing this is that dephasing results in the contribution to the spectra for large values of the interval between interactions with the electric field is smaller than for small values of that interval. Therefore, the average can be used in the first place. However, it seems more reasonable that the contribution from the Hamiltonian at long intervals should decrease slowly than assuming a sudden drop at one specific time T, as proposed in the original approach. We will furthermore introduce a forward and a backward average. The reason for this generalization becomes obvious when we consider the 2DIR response.

Using the time-averaging approximation the linear absorption is given by[25]

$$I(\omega) = \Im \sum_n \left\langle [\mu_n^F(0)]^2 \frac{1}{\epsilon_n^F(0) - \omega + i\gamma} \right\rangle. \tag{5}$$

Here $\epsilon_n^F(0)$ is the nth eigenfrequency of the forward average Hamiltonian and $\mu_n^F(0)$ is the corresponding transition dipole. γ is the width of the homogeneous line broadening arising due to the vibrational lifetime, $\gamma = 1/2T_1$.

For practical purposes the trajectory of the Hamiltonian is recorded in snapshots separated by equidistant time intervals Δt. The forward average for the pth snapshot is given by

$$H^F(p\Delta t) = \sum_{q=0}^{[\tau_C/\Delta t]} H[(p+q)\Delta t] W(q\Delta t)\Delta t. \tag{6}$$

The $[\cdots]$ above the summation denotes the integer value of the argument. Given a trajectory with M snapshots the forward average can be generated for snapshots with $0 \leq p < M - [\tau_C/\Delta t]$. The backward average is given by

$$H^B(p\Delta t) = \sum_{q=0}^{[\tau_C/\Delta t]} H[(p-q)\Delta t] W(q\Delta t)\Delta t. \tag{7}$$

This can be generated for snapshots with $[\tau_C/\Delta t] \leq p < M$. $W(t)$ is an appropriate weight function and τ_C is a time cutoff introduced for practical reasons. The weight function fulfills the normalization requirement

$$\sum_{q=0}^{[\tau_C/\Delta t]} W(q\Delta t)\Delta t = 1. \tag{8}$$

The time averaging is performed numerically in all simulations by summing over contributions from different snapshots along the trajectories as given by Eqs. (6) and (7).

The excited state absorption is the most complex and time consuming contribution to calculate

$$S_{\mathrm{EA}}^{(3)}(t_1,t_2,t_3) = \sum_{j,k,l,m,n,p} \exp[-(t_1+2t_2+t_3)/2T_1 - t_3/2T_1'] \times \langle \mu_p(\tau_2) U_{pj}(\tau_2,\tau_S)\mu_{jk}(\tau_S) U_{kl}(\tau_S,\tau_3)\mu_{lm}(\tau_3) U_{mn}(\tau_3,\tau_1)\mu_n(\tau_1)\rangle$$
$$+ \langle \mu_p(\tau_1) U_{pj}(\tau_1,\tau_S)\mu_{jk}(\tau_S) U_{kl}(\tau_S,\tau_3)\mu_{lm}(\tau_3) U_{mn}(\tau_3,\tau_2)\mu_n(\tau_2)\rangle. \tag{9}$$

The lifetime of the double excited state is T_1'. When averaging over many slightly different configurations, the contribution to the signal in the time domain response function decays with the dephasing rate as t_1 and t_3 grows. This is illustrated in Fig. 1. This suggests the use of a weighted average that weights the Hamiltonian corresponding to short t_1 and t_3 higher. We derive the expression for the excited state absorption contribution to the 2DIR response in the time-averaging approximation in Appendix B. The derivation of the ground state bleach and stimulated emission contributions can be done in an analogous way.

The stimulated emission is given by the rephasing and nonrephasing contributions

$$I_{\mathrm{SE}}^{(1)}(\omega_1,t_2,\omega_3) = -\sum_{j,k,l,n} \left\langle \frac{1}{-\epsilon_n^B(0) - \omega_1 + i\gamma} \frac{1}{\epsilon_j^F(t_2) - \omega_3 + i\gamma} \mu_n^B(0)\mu_k^B(0)\mu_j^F(t_2)\mu_l^F(t_2) U_{nl}^{FB}(-t_2) U_{jk}^{FB}(t_2) \right\rangle \times \exp(-t_2/T_1) \tag{10}$$

$$I_{\mathrm{SE}}^{(\mathrm{II})}(\omega_1,t_2,\omega_3) = -\sum_{j,k,l,n}\left\langle \frac{1}{\epsilon_n^B(0)-\omega_1+i\gamma}\frac{1}{\epsilon_j^F(t_2)-\omega_3+i\gamma}\mu_n^B(0)\mu_k^B(0)\mu_j^F(t_2)\mu_l^F(t_2)U_{lk}^{FB}(-t_2)U_{jn}^{FB}(t_2)\right\rangle \times \exp(-t_2/T_1). \quad (11)$$

Here $\epsilon_j^B(0)$ are the eigenvalues of the backward time-average Hamiltonian at time 0, $H^B(0)$, and $\epsilon_j^F(t_2)$ are the eigenvalues of the forward time-average Hamiltonian at time t_2, $H^F(t_2)$. These time-average Hamiltonians are found numerically by applying Eqs. (6) and (7) to the trajectory of Hamiltonian snapshots. $\mu_n^B(0)$ is the transition dipole for eigenstate n of the backward average Hamiltonian at time 0, and $\mu_n^F(t_2)$ is the transition dipole for eigenstate n of the forward average Hamiltonian at time t_2. $U_{jn}^{FB}(t_2)$ and $U_{lk}^{FB}(-t_2)$ are matrix elements of the time evolution operator transformed in such a way, that the rows are in the basis of the forward average eigenstates and the columns are the backward average eigenstates. The time evolution operators are obtained by numerical integration of the time-dependent Schrödinger equation using the Hamiltonian from Eq. (1) as described in Ref. 21. For simplicity polarization dependence is omitted in the expressions for the contributions to the 2DIR spectra. The dipoles are therefore written as scalars. The sum over all possible Cartesian coordinates and averaging over polarization components of the transition dipole vectors as described in Ref. 37 is understood to be implicit.

The excited state absorption is given by the rephasing and nonrephasing contributions

$$I_{\mathrm{EA}}^{(\mathrm{I})}(\omega_1,t_2,\omega_3) = \sum_{j,k,l,n}\left\langle \frac{1}{-\epsilon_n^B(0)-\omega_1+i\gamma}\frac{1}{\epsilon_m^F(t_2)-\epsilon_l^F(t_2)-\omega_3+i(\gamma+\gamma')}\mu_n^B(0)\mu_k^B(0)\mu_{mj}^F(t_2)\mu_{ml}^F(t_2)U_{\ln}^{FB}(-t_2)U_{jk}^{FB}(t_2)\right\rangle \times\exp(-t_2/T_1), \quad (12)$$

$$I_{\mathrm{EA}}^{(\mathrm{II})}(\omega_1,t_2,\omega_3) = \sum_{j,k,l,n}\left\langle \frac{1}{\epsilon_n^B(0)-\omega_1+i\gamma}\frac{1}{\epsilon_m^F(t_2)-\epsilon_l^F(t_2)-\omega_3+i(\gamma+\gamma')}\mu_n^B(0)\mu_k^B(0)\mu_{mj}^F(t_2)\mu_{ml}^F(t_2)U_{lk}^{FB}(-t_2)U_{jn}^{FB}(t_2)\right\rangle \times\exp(-t_2/T_1). \quad (13)$$

The homogenous broadening arising from the double excited state lifetime $\gamma'=1/2T_1'$ is set to zero in the present simulations for simplicity.

The ground state bleach is given by the rephasing and nonrephasing contributions

$$I_{\mathrm{GB}}^{(\mathrm{I})}(\omega_1,t_2,\omega_3) = -\sum_{j,n}\left\langle \frac{1}{-\epsilon_n^B(0)-\omega_1+i\gamma}\frac{1}{\epsilon_j^F(t_2)-\omega_3+i\gamma}[\mu_n^B(0)\mu_j^F(t_2)]^2\right\rangle \exp(-t_2/T_G), \quad (14)$$

$$I_{\mathrm{GB}}^{(\mathrm{II})}(\omega_1,t_2,\omega_3) = -\sum_{j,n}\left\langle \frac{1}{+\epsilon_n^B(0)-\omega_1+i\gamma}\frac{1}{\epsilon_j^F(t_2)-\omega_3+i\gamma}[\mu_n^B(0)\mu_j^F(t_2)]^2\right\rangle \exp(-t_2/T_G). \quad (15)$$

T_G is the time it takes for the population, excited in the stimulated emission pathway, to decay to the ground state, which will lead to cancellation with the ground state bleach pathway. In the case where the population goes directly to the ground state T_G is equal to the lifetime T_1 otherwise it is larger than the lifetime. For simplicity we will consider $T_G=T_1$. The total spectrum is given by the real part of the sum of the six contributions in Eqs. (10)–(15). In the obtained time-averaging approximation the evolution during the time delays t_1 and t_3 is adiabatic. This means that no coherence transfer can take place between different eigenstates in these time intervals and this effect is thus omitted in Fig. 2.

B. Weight functions

In order to choose a suitable weight function W for the averaging, we tested the three most obvious candidates in the case of one vibration with the frequency fluctuations described by an overdamped Brownian oscillator model. These three weight functions are the exponential function, a box shaped function, and a Gaussian function. For one overdamped Brownian oscillator the frequency correlation function is

$$\langle\omega(t)\omega(0)\rangle = \Delta^2\exp(-\Lambda t), \quad (16)$$

where Δ is the standard deviation of the frequency fluctuations and Λ is inverse time scale. The line shape of the re-

sulting absorption peak is determined by the line broadening parameter $\kappa := \Lambda/\Delta$. The ratio between the width of the absorption peak and the width of the static distribution of frequencies is adequately described by the Padé approximant[36,38]

$$\Gamma(\kappa)/\Gamma_0 = \frac{1 + 1.76\kappa/2.355}{1 + 0.85\kappa + 0.88\kappa^2}. \tag{17}$$

The detailed line shape is given by a Voigt profile which goes to a Gaussian shape in the inhomogeneous limit ($\kappa \ll 1$) and to a Lorentzian shape in the homogeneous limit ($\kappa \gg 1$).[36,38] In the time-averaging approximation scheme for motional narrowing the line shape is always Gaussian, when the original distribution is Gaussian. An exponential weight function provides the following averaged frequency:

$$\omega_{\tau_A}^{\mathrm{EXP}}(t) = \frac{1}{\tau_A}\int_t^\infty \omega(t')\exp[-(t'-t)/\tau_A]dt' \tag{18}$$

and the ratio between the width of the absorption peak and the width of the static distribution of frequencies is given by

$$\Gamma_{\tau_A}^{\mathrm{EXP}}(\kappa)/\Gamma_0 = \sqrt{\frac{1}{\tau_A\Delta\kappa + 1}}. \tag{19}$$

The averaging time τ_A is a free parameter describing the extent of the averaging. Here $\Gamma_0 = 2.355\Delta = 2.355\sqrt{\langle\omega(0)\omega(0)\rangle}$ and $\Gamma_{\tau_A}^{\mathrm{EXP}} = 2.355\sqrt{\langle\omega_{\tau_A}^{\mathrm{EXP}}(0)\omega_{\tau_A}^{\mathrm{EXP}}(0)\rangle}$. With a box weight function the averaged frequency is

$$\omega_{\tau_A}^{\mathrm{BOX}}(t) = \frac{1}{\tau_A}\int_t^{t+\tau_A} \omega(t')dt' \tag{20}$$

and the corresponding ratio between the widths equals

$$\Gamma_{\tau_A}^{\mathrm{BOX}}(\kappa)/\Gamma_0 = \frac{\sqrt{2[\exp(-\kappa\tau_A\Delta) - 1 + \tau_A\Delta\kappa]}}{\kappa\tau_A\Delta}. \tag{21}$$

The width of the box average distribution is given by $\Gamma_{\tau_A}^{\mathrm{BOX}} = 2.355\sqrt{\langle\omega_{\tau_A}^{\mathrm{BOX}}(0)\omega_{\tau_A}^{\mathrm{BOX}}(0)\rangle}$. On the other hand, using a Gaussian weight function, the averaged frequency is given by

$$\omega_{\tau_A}^{\mathrm{GAUSS}}(t) = \frac{2}{\sqrt{2\pi}\tau_A}\int_t^\infty \omega(t')\exp\left[-\frac{1}{2}\left(\frac{t'-t}{\tau_A}\right)^2\right]dt'. \tag{22}$$

In this case the ratio between the width of the absorption peak and the width of the static distribution of frequencies is described by the function

$$\Gamma_{\tau_A}^{\mathrm{GAUSS}}(\kappa)/\Gamma_0 = \sqrt{4\exp(\kappa^2\Delta^2\tau_A^2)[\Phi(-\kappa\Delta\tau_A\sqrt{2}) - \Phi(-\kappa\Delta\tau_A)]}. \tag{23}$$

Here the function $\Phi(x)$ is defined

$$\Phi(x) = \frac{1}{\sqrt{2\pi}}\int_{-\infty}^x \exp\left(-\frac{t^2}{2}\right)dt. \tag{24}$$

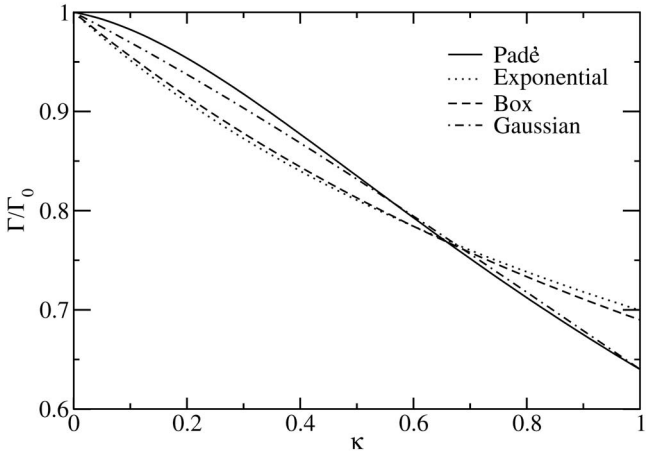

FIG. 3. The linewidths for a Gaussian–Markovian model obtained with the three averaging schemes compared with the linewidth predicted by the Padé approximant.

The value of the averaging time τ_A is in all these schemes a free parameter. However, in the expressions for the linewidth, it is always multiplied with the width of the static frequency distribution. A uniform behavior is therefore obtained if the averaging time is taken to be proportional to the inhomogeneous dephasing time $\tau_D = 1/\Delta$. The optimal proportionality constant was found by fitting Eqs. (19), (21), and (23) to the Padé approximant in the region $0 \le \kappa \le 1$. Therefore, the optimal value for τ_A is $1.04\Delta^{-1}$, $2.79\Delta^{-1}$, and $0.63\Delta^{-1}$ for the exponential, box, and Gaussian weight functions, respectively. The linewidths predicted with those parameters are shown in Fig. 3. The averaging schemes all predict too narrow peaks when the line broadening parameter is between 0 and 0.6. At larger values the predicted linewidths are too broad. The exponential and box schemes predict practically identical linewidths in the investigated range. The Gaussian scheme is considerably better than the two other schemes. The errors in the predicted linewidths are typically below 2% for this scheme, whereas it can be even twice as big in the two other schemes.

III. RESULTS

In the following we will demonstrate the time-averaging approximation. We will use a model in which the two oscillators have the same average frequency of 1050 cm^{-1}. An overdamped stochastic model is used to describe the time dependence of the vibrational frequencies.[35] This is done in such a way that the frequency fluctuations of the two oscillators were uncorrelated. The distribution of the generated frequencies is Gaussian and the autocorrelation functions exponential.[39] The widths of the distributions are set to 20 cm^{-1} corresponding to an inhomogeneous dephasing time of $\tau_D = 265$ fs. Three different time scales are used for the fluctuations $\Lambda^{-1} = 100$, 500, and 2000 fs corresponding to line broadening parameters $\kappa = 2.65$, 0.53, and 0.1325. The two oscillators are coupled with a coupling constant of $J_{12}(t) = J_{12} = 25$ cm^{-1}. The angle between the transition dipoles is fixed at 90°. We fix the anharmonicity for the individual oscillators at 10 cm^{-1}. The vibrational lifetime T_1 was set to 5 ps. The constructed trajectory was 2 ns long with the

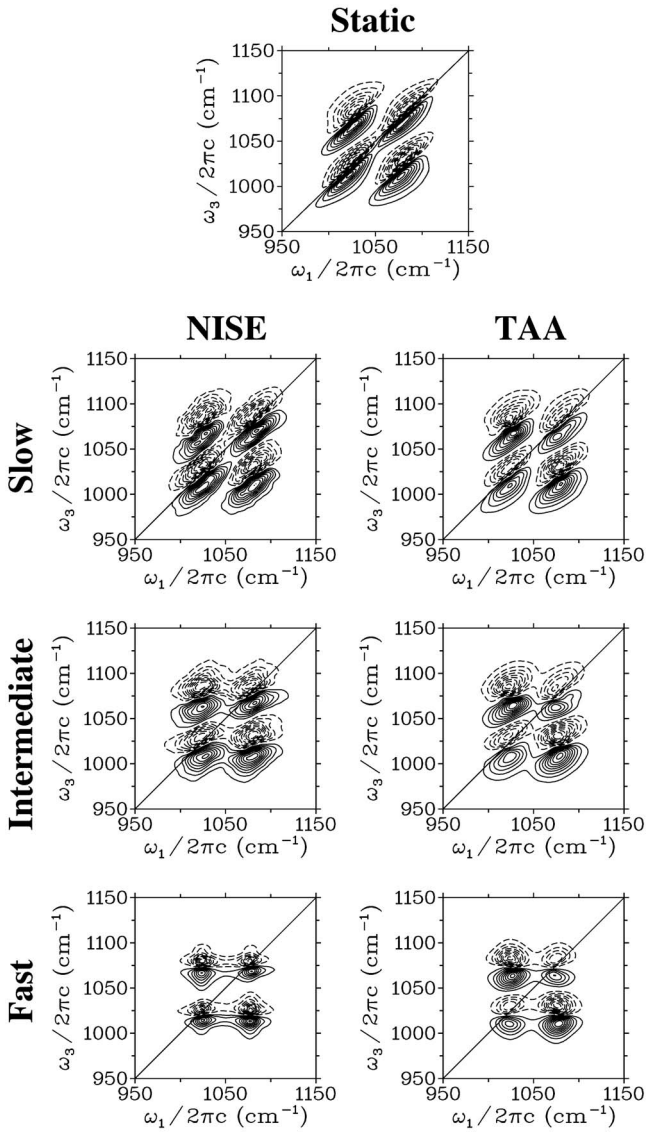

FIG. 4. Top: The spectrum obtained in the static limit, which is identical for the three models with different fluctuation time scales. Left column: the 2DIR spectra for the three models with the numerical integration of the Schrödinger equation method. Right column: The 2DIR spectra for the same three models obtained with the TAA. The contour lines are plotted for every 10% of the maximum signal in each plot but omitting the contour for zero intensity. The dashed lines indicate negative absorption (i.e., ground state bleach and stimulated emission contributions) while full lines indicate positive absorption (excited state absorption contributions).

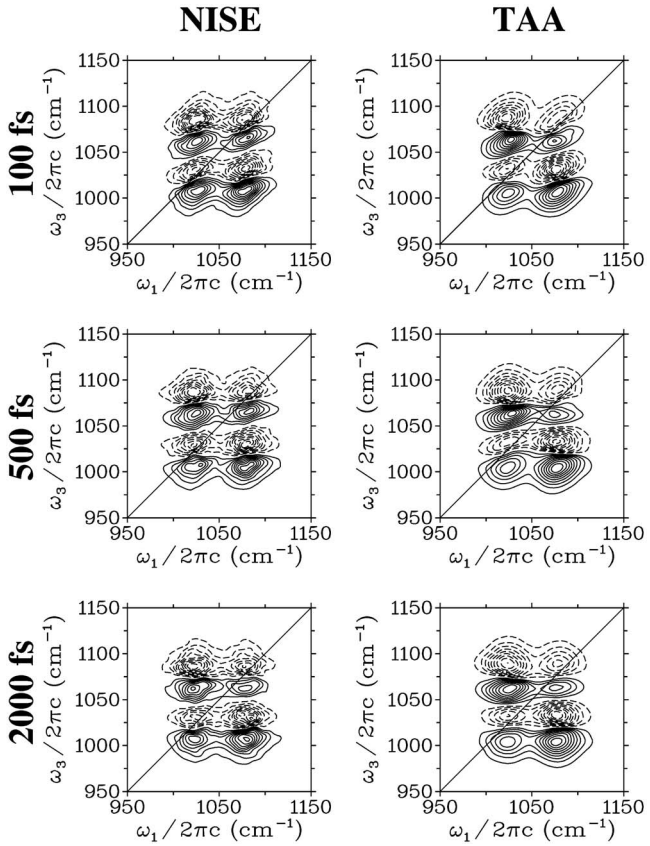

FIG. 5. The two-dimensional infrared spectra with different waiting times for the model with intermediate fluctuation time scale. Left column: the 2DIR spectra for the three models with the numerical integration of the Schrödinger equation method. Right column: The 2DIR spectra for the same three models obtained with the TAA. The contours are drawn as in Fig. 4.

Hamiltonian stored at every 10 fs. We calculated the spectra both with the NISE method and the TAA method. For the TAA method we used a Gaussian weight function with the parameters $\tau_A=0.85\Delta^{-1}$ and $\tau_C=3\tau_A$.

The simulated 2DIR spectra, in the case in which the polarization of the first two laser fields is perpendicular to the polarization of the two last ones, is shown in Fig. 4. In the static approximation the signals are elongated along the diagonal and the width in the antidiagonal direction is solely due to the lifetime broadening. For the slow fluctuations the peaks are still stretched along the diagonal. A slight increase in the antidiagonal linewidth is observed in comparison with the static case. Only slight differences are observed between the NISE and TAA results. For the intermediate fluctuations the peaks start tilting forming an angle with the diagonal line. This feature is clearly observed in both the NISE and TAA spectra. The antidiagonal widths of the peaks are further increased, which is again well described by the approximation. Finally, for the fast fluctuations the node lines between the negative and positive contributions are almost horizontal. The widths of the peaks in the diagonal and antidiagonal directions are practically the same. TAA spectra catch these features very well, but the peaks are clearly rounder than the peaks in the NISE spectrum. This is because the TAA method retains the Gaussian line shape of the peaks, while the correct treatment results in Lorentzian line shapes for fast fluctuations.

We tested the method for different waiting times t_2. In Fig. 5 the spectra calculated with the NISE and TAA methods are shown for the model with $\Lambda^{-1}=500$ fs. Waiting times of 100, 500, and 2000 fs were used. At the shortest waiting time, some correlation between the frequency during t_1 and the frequency during t_3 is still retained. Most of the correlation has gone at 500 fs. At 2000 fs all correlation is practically lost. The NISE and TAA spectra are very similar, with the only difference that the TAA spectra appear slightly broader and have a slightly rounder shape.

The calculations were performed at a 3.4 MHz Intel Linux personal computer. The full calculation took $37\frac{1}{2}$ h, while the time-averaging approximation took 1 min and 45 s.

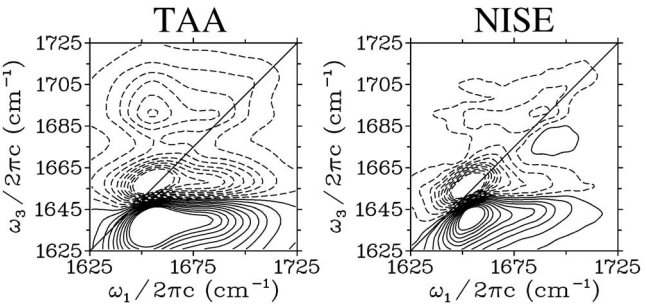

FIG. 6. The 2DIR spectrum of the amide I region for β-hairpin Trpzip2 calculated in the TAA and using the NISE. The contours are drawn as in Fig. 4.

This is a speed-up of more than 1000 times. One could possibly obtain a speed-up of the full calculation by adjusting the algorithm used, but not in the order of magnitude observed with the time-averaging approximation.

We further tested the approximation on the amide I band of the β-hairpin peptide Trpzip2.[40] To do this we used a Hamiltonian generated in a previous study.[24] In that study the initial Trpzip2 structure was taken from the Protein Database (PDB 1LE1) (Ref. 40) and molecular dynamics (MD) simulations with GROMACS-3.1.4.[41] The simulation details are given in Ref. 24. Ten different configurations were generated by the MD simulation with 1 ns between each configuration. For each configuration a 100 ps simulation was performed storing the structure every 20 fs, giving ten trajectories with a total of 50 000 stored snapshots. The Hamiltonian was then constructed using a density functional theory based electrostatic map giving the amide I as a function of the electric field generated by the solvent on the amide unit.[42] The couplings between different units were found using the transition charge coupling scheme.[43] Through bond effects with neighboring units were accounted for using a Ramachandran angle based map.[43] The anharmonicity needed for describing double excited states was set to 16 cm^{-1} on all units.[5] A total of 11 CO amide I modes were included in the simulation.

The spectra calculated with the time-average procedure using a 167 fs averaging time with a Gaussian weight function. This corresponds to an inhomogeneous linewidth of 20 cm^{-1}. The resulting spectrum in the perpendicular polarization configuration is compared with the NISE spectrum in Fig. 6. The basic structure of the spectrum is well reproduced. However, the peaks are generally too broad and the cross peak at $(\omega_1,\omega_1)=(1650\ \text{cm}^{-1},1690\ \text{cm}^{-1})$ is too intense in the TAA calculation. These differences can either be due to the neglect of nonadiabatic effects during the time delays t_1 and t_3 or it might arise because all elements of the Hamiltonian were averaged with the same averaging time. The latter might be a special problem for the fluctuating coupling. It might be possible to improve the agreement by optimizing the averaging procedure for problems where the coupling is fluctuating. The NISE calculation took 100 h, while the TAA calculation took less than a minute on the same computer used for the dimer simulations.

The reason that the time-averaging approximation is so efficient is that the Fourier transform of the time intervals t_1 and t_3 is circumvented. This Fourier transform is in it self not time consuming, however, in order to obtain the desired spectral width and resolution with the NISE approach one needs to calculate the response function for numerous values of t_1 and t_3. In practice 128 or 256 values for each time interval were used for the β-hairpin and the dimer, respectively. This means that hundreds of matrix multiplications are needed for calculating these times, while in the time-averaging approximation the response is calculated directly in the frequency domain and all these matrix multiplications are circumvented. For larger systems the dimension of the matrices involving the double excited states are much larger than the ones involving the single excited states and therefore the loop over t_3 for the excited state absorption becomes the bottleneck.

IV. CONCLUSIONS

In the present paper, we calculated the linewidth that is obtained when averaging over the fluctuating frequency using different weight functions for overdamped Brownian fluctuations. The averaging procedure introduces a free parameter, an averaging time τ_A, for each of the possible weighting functions. We optimized the free parameter by fitting to the Padé approximant that gives a very good description of the linewidth for the overdamped Brownian model. We found that, at least for this commonly occurring case, the Gaussian weight function gave the best results over a broad range of fluctuation time scales.

We further extended the time-averaging approximation to allow the calculation of the two-dimensional infrared signal. The approximation does this in a way accounting for both motional narrowing during the time intervals t_1 and t_3 and population dynamics and spectral diffusion during the waiting time t_2. The approximation catches the most important spectral features. These are the homogeneous line broadening observed in the antidiagonal direction, the motional narrowing observed in the diagonal direction, and finally the tilt of the node lines between the negative and positive peaks. The spectral changes observed with varying waiting time t_2 were also reproduced. The approximation as contemplated does not account for the change of the peak shapes from Gaussian to Lorentzian ones for fast fluctuations. The approximation preserves the Gaussian shape. In cases where the nonadiabatic coupling is so strong that it plays a significant role during the time intervals t_1 and t_3, one expects the TAA to breakdown because it does not account for coherence transfer in those time periods. The two involved vibrations had identical static frequency distributions and a fixed coupling in the dimer model example. When this is the case, a solution could be to use different averaging times τ_A for different matrix elements in the Hamiltonian. The cross peak got too much intensity and the lines were too broad in the Trpzip2 β-hairpin simulation. This is most likely resulting from either nonadiabatic effects or the fact that here the coupling is fluctuating, and we used the same averaging procedure for all elements of the Hamiltonian.

The time-averaging approximation catches the most important dynamical effects that are completely lost in the static approximation, and it is significantly faster than the

full calculation with the numerical integration of the Schrödinger equation and comparable in speed to the static approximation. This provides the time-averaging approximation as a promising efficient approximate method for fitting experimental spectra and calculating the spectra of large dynamical systems as the OH-stretch band in liquid water and the amide vibrations of large proteins.

ACKNOWLEDGMENTS

One of the authors (T.l.C.J.) acknowledges the Netherlands Organization for Scientific Research (NWO) for support through a VENI grant. The authors thank Professor A. Tokmakoff, Professor J. Knoester, and Professor A. C. D. van Enter for helpful discussions.

APPENDIX A: THE AVERAGED LINEWIDTH IN THE GAUSSIAN MARKOVIAN APPROXIMATION

The two-point correlation function with respect to the Gaussian weight function and averaging time τ_A is given by

$$\left\langle \omega_{\tau_A}^{\mathrm{GAUSS}}(0)\omega_{\tau_A}^{\mathrm{GAUSS}}(0)\right\rangle = \frac{2}{\sqrt{2\pi}\tau_A}\frac{2}{\sqrt{2\pi}\tau_A} \times \int_0^\infty \int_0^\infty e^{-\Lambda|t-t'|}e^{-1/2(t/\tau_A)^2}e^{-1/2(t'/\tau_A)^2}dtdt'. \quad \text{(A1)}$$

With a change in variables $t/\tau_A \to t$, respectively, $t'/\tau_A \to t'$, we obtain that Eq. (A1) is equal to

$$\frac{2}{\sqrt{2\pi}}\frac{2}{\sqrt{2\pi}}\int_0^\infty \int_0^\infty e^{-\Lambda\tau_A|t-t'|}e^{-(1/2)t^2}e^{-(1/2)(t')^2}dtdt'.$$

Since the function we want to integrate is symmetric under reflection we can rewrite the former integral as

$$2\frac{1}{\sqrt{2\pi}}\frac{1}{\sqrt{2\pi}}\int_{-\infty}^\infty \int_{-\infty}^\infty e^{-\Lambda\tau_A|t-t'|}e^{-(1/2)t^2}e^{-(1/2)(t')^2}dtdt' - 4\frac{1}{\sqrt{2\pi}}\frac{1}{\sqrt{2\pi}}\int_0^\infty \int_0^\infty e^{-\Lambda\tau_A(t+t')}e^{-(1/2)t^2}e^{-(1/2)(t')^2}dtdt'. \quad \text{(A2)}$$

The first integral can be seen as

$$2\langle e^{-\Lambda\tau_A|X|}\rangle = 2\frac{1}{\sqrt{4\pi}}\int_{-\infty}^\infty e^{-\Lambda\tau_A|x|}e^{-x^2/4}dx = 4\frac{1}{\sqrt{4\pi}}\int_0^\infty e^{-\Lambda\tau_A x}e^{-x^2/4}dx,$$

that is the expectation of an exponential of the absolute value of a Gaussian random variable X with mean 0 and variance 2. After some algebraic manipulations we get that

$$2\langle e^{-\Lambda\tau_A|X|}\rangle = 4e^{\Lambda^2\tau_A^2}\int_{-\infty}^{-\sqrt{2}\Lambda\tau_A}\frac{1}{\sqrt{2\pi}}e^{-x^2/2}dx,$$

which we can write as $4e^{\Lambda^2\tau_A^2}\Phi(-\sqrt{2}\Lambda\tau_A)$, where $\Phi(x)$ is the error function defined as

$$\Phi(x) = \frac{1}{\sqrt{2\pi}}\int_{-\infty}^x e^{-t^2/2}dt.$$

The second integral in Eq. (A2) can be factorized as

$$\frac{2}{\sqrt{2\pi}}\frac{2}{\sqrt{2\pi}}\int_0^\infty \int_0^\infty e^{-\Lambda\tau_A(t+t')}e^{-(1/2)t^2}e^{-(1/2)(t')^2}dtdt' = \left(\frac{2}{\sqrt{2\pi}}\int_0^\infty e^{-\Lambda\tau_A t}e^{-(1/2)t^2}dt\right) \times \left(\frac{2}{\sqrt{2\pi}}\int_0^\infty e^{-\Lambda\tau_A t'}e^{-(1/2)(t')^2}dt'\right). \quad \text{(A3)}$$

The integrals in the brackets are simply equal to

$$\frac{2}{\sqrt{2\pi}}\int_0^\infty e^{-\Lambda\tau_A t'}e^{-(1/2)(t')^2}dt' = 2e^{\Lambda^2\tau_A^2}\Phi(-\Lambda\tau_A)$$

and therefore the right-hand side of Eq. (A3),

$$4e^{\Lambda^2\tau_A^2}\Phi^2(-\Lambda\tau_A).$$

In summary we have found the explicit expression for the two-point correlation function

$$\langle \omega_{\tau_A}^{\mathrm{GAUSS}}(0)\omega_{\tau_A}^{\mathrm{GAUSS}}(0)\rangle = 4e^{\Lambda^2\tau_A^2}[\Phi(-\sqrt{2}\Lambda\tau_A) - \Phi^2(-\Lambda\tau_A)].$$

APPENDIX B: THE TIME-AVERAGING APPROXIMATION FOR 2DIR

In order to obtain the time-averaging expression for the 2DIR response we need to rewrite the response function Eq. (9) in a way that collects the time intervals t_1 and t_3. For the excited state absorption we get

$$S_{\mathrm{EA}}^{(3)}(t_1,t_2,t_3) = \sum_{j,k,l,m,n,p} \exp[-(t_1+2t_2+t_3)/2T_1 - t_3/2T_1'] \quad \text{(B1)}$$

$$\times\langle \mu_{jk}(\tau_S)\mu_{lm}(\tau_3)\mu_n(\tau_1)\mu_p(\tau_2)U_{kl}(\tau_S,\tau_3)U_{mn}(\tau_3,\tau_1) \times U_{pj}(\tau_2,\tau_S)\rangle \quad \text{(B2)}$$

$$+\langle \mu_{jk}(\tau_S)\mu_{lm}(\tau_3)\mu_n(\tau_1)\mu_p(\tau_2)U_{kl}(\tau_S,\tau_3) \times U_{mn}(\tau_3,\tau_2)U_{pj}(\tau_1,\tau_S)\rangle. \quad \text{(B3)}$$

We now use that the time evolution operators can be split, i.e.,

$$U_{pj}(\tau_2,\tau_S) = \sum_q U_{pq}(\tau_2,\tau_3)U_{qj}(\tau_3,\tau_S). \quad \text{(B4)}$$

This leads to the expression

$$S^{(3)}_{\mathrm{EA}}(t_1,t_2,t_3) = \sum_{j,k,l,m,n,p,q,r} \exp[-(t_1+2t_2+t_3)/2T_1 - t_3/2T_1'] \times \langle \mu_{jk}(\tau_S)\mu_{lm}(\tau_3)\mu_n(\tau_1)\mu_p(\tau_2)U_{kl}(\tau_S,\tau_3)U_{mq}(\tau_3,\tau_2)U_{qn}(\tau_2,\tau_1)U_{pr}(\tau_2,\tau_3)U_{rj}(\tau_3,\tau_S)\rangle + \langle \mu_{jk}(\tau_S)\mu_{lm}(\tau_3)\mu_n(\tau_1)\mu_p(\tau_2)U_{kl}(\tau_S,\tau_3)U_{mn}(\tau_3,\tau_2)U_{pq}(\tau_1,\tau_2)U_{qr}(\tau_2,\tau_3)U_{rj}(\tau_3,\tau_S)\rangle. \quad \text{(B5)}$$

We now make the time-averaging approximation and replace the time evolution operators involving τ_1 and τ_2 with the backward average time evolution operator

$$U^B_{jk}(\tau_2,\tau_1) = \left\{ \exp\left[-\frac{i(\tau_2-\tau_1)}{\hbar}\int_{\tau_2}^{-\infty} \boldsymbol{H}(t)w(\tau_2-t)dt \right] \right\}_{jk}. \quad \text{(B6)}$$

Similarly, the time evolution operators involving τ_S and τ_3 are replaced with the forward average time evolution operator

$$U^F_{jk}(\tau_S,\tau_3) = \left\{ \exp\left[-\frac{i(\tau_S-\tau_3)}{\hbar}\int_{\tau_3}^{-\infty} \boldsymbol{H}(t)w(t-\tau_3)dt \right] \right\}_{jk}. \quad \text{(B7)}$$

This provides the expression

$$S^{(3)}_{\mathrm{EA}}(t_1,t_2,t_3) = \sum_{j,k,l,m,n,p,q,r} \exp[-(t_1+2t_2+t_3)/2T_1 - t_3/2T_1'] \times \langle \mu_{jk}(\tau_S)\mu_{lm}(\tau_3)\mu_n(\tau_1)\mu_p(\tau_2)U^F_{kl}(\tau_S,\tau_3)U^F_{rj}(\tau_3,\tau_S)U_{mq}(\tau_3,\tau_2)U^B_{qn}(\tau_2,\tau_1)U_{pr}(\tau_2,\tau_3)\rangle + \langle \mu_{jk}(\tau_S)\mu_{lm}(\tau_3)\mu_n(\tau_1)\mu_p(\tau_2)U^F_{kl}(\tau_S,\tau_3)U^F_{rj}(\tau_3,\tau_S)U_{mn}(\tau_3,\tau_2)U^B_{pq}(\tau_1,\tau_2)U_{qr}(\tau_2,\tau_3)\rangle. \quad \text{(B8)}$$

We now change from the site basis used so far. At times τ_1 and τ_2 we use the eigenbasis of the backward average Hamiltonian $[H^B(\tau_2)]$ and at τ_3 and τ_S we use the eigenbasis of the forward average Hamiltonian $[H^F(\tau_3)]$. The transformed dipoles are denoted μ^F and μ^B, respectively. The time evolution operators for the time delay t_2 are transformed to the t_1 eigenbasis at one side and the t_3 eigenbasis at the other. The time evolution during this time delay is then governed by the transformed operator

$$U^{FB}_{ji}(t_2) = \sum_{pq} c^{\dagger}_{jp}(t_3)U_{pq}(\tau_3,\tau_2)c_{qj}(t_1). \quad \text{(B9)}$$

Here $c^F_{jp}(t_3)$ and $c^B_{qj}(t_1)$ are the operators diagonalizing the Hamiltonians during t_3 and t_1, respectively. The 2DIR response for the excited state emission is then

$$S^{(3)}_{\mathrm{EA}}(t_1,t_2,t_3) = \sum_{j,k,l,m,n,p,q,r} \exp[-(t_1+2t_2+t_3)/2T_1 - t_3/2T_1'] \times \langle \mu^F_{jk}(\tau_3)\mu^F_{lm}(\tau_3)\mu^B_n(\tau_1)\mu^B_p(\tau_2)U^F_{kl}(\tau_S,\tau_3)U^F_{rj}(\tau_3,\tau_S)U^{FB}_{mq}(t_2)U^B_{qn}(\tau_2,\tau_1)U^{FB}_{pr}(-t_2)\rangle + \langle \mu^F_{jk}(\tau_S)\mu^F_{lm}(\tau_3)\mu^B_n(\tau_1)\mu^B_p(\tau_2)U^F_{kl}(\tau_S,\tau_3)U^F_{rj}(\tau_3,\tau_S)U^{FB}_{mn}(t_2)U^B_{pq}(\tau_1,\tau_2)U^{FB}_{qr}(-t_2)\rangle. \quad \text{(B10)}$$

The time-averaging time-evolution operators U^B and U^F are now diagonal, which allow a reduction in the number of summation indices. Furthermore, the Fourier transforms of the time delays t_1 and t_3 are now trivial giving Lorentzians depending on the eigenvalues and the lifetime damping $\gamma = 1/2T_1$ and $\gamma' = 1/2T_1'$. We then reach the final expression for the excited state absorption contribution to the 2DIR response

$$I^{(\mathrm{I})}_{\mathrm{EA}}(\omega_1,t_2,\omega_3) = \sum_{j,k,l,m,n} \left\langle \frac{1}{-\epsilon^B_n(0)-\omega_1+i\gamma} \frac{1}{\epsilon^F_m(t_2)-\epsilon^F_l(t_2)-\omega_3+i(\gamma+\gamma')} \mu^B_n(0)\mu^B_k(0)\mu^F_{mj}(t_2)\mu^F_{ml}(t_2) \times U^{FB}_{ln}(-t_2)U^{FB}_{jk}(t_2) \right\rangle \times \exp(-t_2/T_1) \quad \text{(B11)}$$

$$+ \sum_{i,j,k,l,n} \left\langle \frac{1}{\epsilon^B_n(0)-\omega_1+i\gamma} \frac{1}{\epsilon^F_m(t_2)-\epsilon^F_l(t_2)-\omega_3+i(\gamma+\gamma')} \mu^B_n(0)\mu^B_k(0)\mu^F_{mj}(t_2)\mu^F_{ml}(t_2) \times U^{FB}_{lk}(-t_2)U^{FB}_{jk}(t_2) \right\rangle \exp(-t_2/T_1). \quad \text{(B12)}$$

The derivation of the ground state bleach and stimulated emission contributions follow the exact same steps as that of the excited state absorption. All the contributions are given in Eqs. (10)–(15). The absorptive spectrum is given by the real part of the response function.

[1] N. Koumura, R. Zijlstra, R. van Delden, H. Harada, and B. Feringa, Nature (London) **401**, 152 (1999).
[2] E. Buhleier, W. Wehner, and F. Vögtle, Synthesis **1978**, 155 (1978).
[3] W. Kuhlbrandt and D. Wang, Nature (London) **350**, 6314 (1991).
[4] S. Mukamel, Annu. Rev. Phys. Chem. **51**, 691 (2000).
[5] P. Hamm, M. H. Lim, and R. M. Hochstrasser, J. Phys. Chem. B **102**, 6123 (1998).
[6] D. M. Jonas, Annu. Rev. Phys. Chem. **54**, 425 (2003).
[7] Y. Tanimura and S. Mukamel, J. Chem. Phys. **99**, 9496 (1993).
[8] J. C. Wright, Int. Rev. Phys. Chem. **21**, 185 (2002).
[9] J. Bredenbeck, J. Helbing, A. Sieg, T. Schrader, W. Zinth, C. Renner, R. Behrendt, L. Moroder, J. Wachtveit, and P. Hamm, Proc. Natl. Acad. Sci. U.S.A. **100**, 6452 (2003).
[10] H. S. Chung, M. Khalil, A. W. Smith, Z. Ganim, and A. Tokmakoff, Proc. Natl. Acad. Sci. U.S.A. **102**, 612 (2005).
[11] S. Woutersen, Y. Mu, G. Stock, and P. Hamm, Proc. Natl. Acad. Sci. U.S.A. **98**, 11254 (2001).
[12] J. Zheng, K. Kwak, J. B. Asbury, X. Chen, I. R. Piletic, and M. D. Fayer, Science **309**, 1338 (2005).
[13] O. F. A. Larsen, P. Bodis, W. J. Buma, J. S. Hannam, D. A. Leigh, and S. Woutersen, Proc. Natl. Acad. Sci. U.S.A. **102**, 13378 (2005).
[14] M. L. Cowan, B. D. Bruner, N. Huse, J. R. Dwyer, B. Chugh, E. T. J. Nibbering, T. Elsaesser, and R. J. D. Miller, Nature (London) **434**, 199 (2005).
[15] N. Demirdöven, C. M. Cheatum, H. S. Chung, M. Khalil, J. Knoester, and A. Tokmakoff, J. Am. Chem. Soc. **126**, 7981 (2004).
[16] J. J. Loparo, S. T. Roberts, and A. Tokmakoff, J. Chem. Phys. **125**, 194522 (2006a).
[17] W. Zhuang, D. Abramavicius, T. Hayashi, and S. Mukamel, J. Phys. Chem. B **110**, 3362 (2006).
[18] S. Mukamel and D. Abramavicius, Chem. Rev. **104**, 2073 (2004).
[19] J.-H. Choi, H. Lee, K.-K. Lee, S. Hahn, and M. Cho, J. Chem. Phys. **126**, 045102 (2007).
[20] H. Torii, Chem. Phys. Lett. **414**, 417 (2005).
[21] T. la Cour Jansen and J. Knoester, J. Phys. Chem. B **110**, 22910 (2006a).
[22] T. la Cour Jansen, W. Zhuang, and S. Mukamel, J. Chem. Phys. **121**, 10577 (2004).
[23] R. D. Gorbunov, P. H. Nguyen, M. Kobus, and G. Stock, J. Chem. Phys. **126**, 054509 (2007).
[24] T. la Cour Jansen and J. Knoester, Biophys. J. **94**, 1818 (2008).
[25] B. M. Auer and J. L. Skinner, J. Chem. Phys. **127**, 104105 (2007).
[26] L. Ojamäe, J. Tegenfeldt, J. Lindgren, and K. Hermansson, Chem. Phys. Lett. **195**, 97 (1992).
[27] A. Ishizaki and Y. Tanimura, J. Chem. Phys. **125**, 084501 (2006).
[28] A. Ishizaki and Y. Tanimura, J. Phys. Chem. A **111**, 9269 (2007).
[29] P. Kjellberg, B. Brüggeman, and T. Pullerits, Phys. Rev. B **74**, 024303 (2006).
[30] S. Mukamel, Phys. Rev. A **28**, 3480 (1983).
[31] K. Hyeon-Deuk, Y. Tanimura, and M. Cho, J. Chem. Phys. **127**, 075101 (2007).
[32] F. Sanda and S. Mukamel, J. Chem. Phys. **125**, 014507 (2006).
[33] M. F. DeCamp, L. DeFlores, J. M. McCracken, A. Tokmakoff, K. Kwac, and M. Cho, J. Phys. Chem. B **109**, 11016 (2005).
[34] J. J. Loparo, S. T. Roberts, and A. Tokmakoff, J. Chem. Phys. **125**, 194521 (2006b).
[35] T. la Cour Jansen and J. Knoester, J. Chem. Phys. **127**, 234502 (2007).
[36] S. Mukamel, *Principles of Nonlinear Optical Spectroscopy* (Oxford University Press, New York, 1995).
[37] R. M. Hochstrasser, Chem. Phys. **266**, 273 (2001).
[38] Y. J. Yan and S. Mukamel, J. Chem. Phys. **89**, 5160 (1988).
[39] D. Cringus, T. la Cour Jansen, M. S. Pshenichnikov, and D. A. Wiersma, J. Chem. Phys. **127**, 084507 (2007).
[40] A. G. Cochran, N. J. Skelton, and M. A. Starovasnik, Proc. Natl. Acad. Sci. U.S.A. **98**, 5578 (2001).
[41] H. J. C. Berendsen, D. van der Spoel, and R. van Drunen, Comput. Phys. Commun. **91**, 43 (1995).
[42] T. la Cour Jansen and J. Knoester, J. Chem. Phys. **124**, 044502 (2006b).
[43] T. la Cour Jansen, A. G. Dijkstra, T. M. Watson, J. D. Hirst, and J. Knoester, J. Chem. Phys. **125**, 044312 (2006).